

Binary matter-wave compactons induced by inter-species scattering length modulations

F. Kh. Abdullaev^{1,2‡}, M.S.A. Hadi¹, Mario Salerno³ and B.A. Umarov¹

¹ Department of Physics, Kulliyah of Science, International Islamic University Malaysia, 25200, Kuantan, Malaysia.

² CCNH, Universidade Federal do ABC, 09210-170, Santo André, Brazil.

³ Dipartimento di Fisica “E.R. Caianiello”, CNISM and INFN - Gruppo Collegato di Salerno, Università di Salerno, Via Giovanni Paolo II, 84084 Fisciano (SA), Italy.

Abstract. Binary mixtures of quasi one-dimensional Bose-Einstein condensates (BEC) trapped in deep optical lattices (OL) in the presence of periodic time modulations of the inter-species scattering length, are investigated. We adopt a mean field description and use the tight binding approximation and the averaging method to derive averaged model equations in the form of two coupled discrete nonlinear Schrödinger equations (DNLSE) with tunneling constants that nonlinearly depend on the inter-species coupling. We show that for strong and rapid modulations of the inter-species scattering length, the averaged system admits exact compacton solutions, e.g. solutions that have no tails and are fully localized on a compact which are achieved when the densities at the compact edges are in correspondence with zeros of the Bessel function (zero tunneling condition). Deviations from exact conditions give rise to the formation of quasi-compactons, e.g. non exact excitations which look as compactons for any practical purpose, for which the zero tunneling condition is achieved dynamically thanks to an effective nonlinear dispersive coupling induced by the scattering length modulation. Stability properties of compactons and quasi-compactons are investigated by linear analysis and by numerical integrations of the averaged system, respectively, and results compared with those from the original (unaveraged) system. In particular, the occurrence of delocalizing transitions with existence of thresholds in the mean inter-species scattering length is explicitly demonstrated. Under proper management conditions, stationary compactons and quasi-compactons are quite stable and robust excitations that can survive on very long time scale. A parameter design and a possible experimental setting for observation of these excitations are briefly discussed.

PACS numbers: 67.85.Hj, 03.75.Kk, 03.75.Lm, 03.75.Nt

‡ Corresponding author: fatkhulla@iium.edu.my

1. Introduction

Localized nonlinear waves with a compact support, so called compactons, are recently attracting interest mainly from mathematical and theoretical points of view. Their existence was predicted for equations of the KdV type with nonlinear dispersion [1] and later demonstrated for several continuous [2] and discrete nonlinear systems in one and two spatial dimensions [3, 4]. In spite of the many investigations, however, they are presently still unobserved in physical experiments. From this point of view appears particularly interesting the theoretical work done on compactons of the discrete nonlinear Schrödinger equation (DNLSE), a model that is linked to physical systems such as nonlinear optical waveguides arrays and Bose-Einstein condensates (BEC) trapped in deep optical lattices (OL). In these contexts, it has been demonstrated that when subjected to periodic time dependent rapid modulations of the nonlinearity, also called strong nonlinearity management (SNM) limit, the DNLSE can support stable compactons of different types [5, 6, 7]. In particular, the existence of one-dimensional compactons in BEC arrays [5] and in binary BEC mixtures with time modulated *intra-species* scattering length [6], as well as, the existence of compactons and vortex-compactons (e.g. vortices on a compact support) in two-dimensional DNLSE [7], were recently demonstrated.

From a physical point of view the existence of compactons is a direct consequence of the tunneling suppression across the edges of the excitation. This phenomenon originates from the nonlinear dispersion term which introduces a dependence of the tunneling constant on the density imbalance between adjacent sites, so that for imbalances matching proper values the tunneling becomes locally suppressed [8, 9]. Experimentally, this phenomenon has been recently observed in BEC in deep OL with periodic time modulations of the interactions [10]. We also remark that the SNM of the scattering lengths is presently used to investigate several interesting physical phenomena related to new quantum phases [11, 12], artificial gauge fields and spin-orbit couplings [13, 14], in BEC systems.

The aim of the present paper is to study binary mixtures of quasi one-dimensional Bose-Einstein condensates in deep optical lattices in the presence of periodic modulations of the *inter-species* scattering length. In this respect, we derive an effective fast time-averaged vector DNLS equation and show that compactons obtained in this case depend on a nonlinear rescaling of the tunneling constants that involves directly the coupling of the two components. In the SNM limit this leads to stable binary compacton solutions with different properties from the ones obtained under an *intra-species* management of the scattering length. More specifically, we show that in addition to the stationary compactons achieved when the edge amplitudes are in correspondence with zeros of the Bessel function (zero tunneling condition), there exist also stationary quasi-compactons for which the zero tunneling condition is achieved dynamically, via the effective coupling induced by the interspecies scattering length modulation. These solutions exist and are stable on a long time scale especially when one of the two

components (say the first) matches the zero tunneling condition in the uncoupled limit, while the other slightly deviates from it. Quite interestingly, we find that for fixed deviations of the amplitude of the second component from a zero of the Bessel function, there exists a threshold for the mean inter-species scattering length above which the zero tunneling condition can be dynamically established for both components and stationary quasi-compactons can exist. For inter-species scattering lengths below the existence threshold, the component matching the zero tunneling condition (in the uncoupled limit) remains alive while the other quickly decays to zero, this leading to the destruction of the binary compacton. As the deviation, for fixed system parameters, from the zero tunneling condition of the inexact component is reduced, the existence threshold moves toward smaller values and completely disappear when the deviation become smaller than a critical value. In the last case it becomes possible to have long living stationary quasi-compactons even if the mean inter-species scattering length is detuned to zero. The solutions predicted by our analysis are checked by means of direct numerical simulations of the full vector DNLS with inter-species scattering length management. The comparison between analytical and numerical results shows a very good agreement in all the investigated cases.

The paper is organized as follows. In Sec. 2 we introduce the model equations for binary a BEC mixtures and use the averaging method to derive the effective equations valid in the limit of strong modulations of the interspecies scattering length. In Sec. 3 we use the averaging equations to investigate the existence and the stability of exact stationary bright-bright compactons localized on one, two and three lattice sites and compare results with the ones obtained from direct numerical integrations of the original (unaveraged) system. In Sec. 4 we consider stationary quasi-compactons for which the condition of the zero tunneling at the compacton edges is dynamically achieved through the inter-species coupling of the BEC mixture. In the last section we discuss physical parameters for possible experimental observations and briefly summarize the main results of the paper.

2. Model equations and averaging

The model equations for a BEC mixture in a one-dimensional (1D) geometry can be derived from a more general three-dimensional formalism by considering a trapping potential with the transversal frequency ω_{\perp} much larger than the longitudinal frequency ω_{\parallel} , e.g. $\omega_{\perp} \gg \omega_{\parallel}$. In the present case, the trap potential in the x -direction is an OL generated by two counter-propagating laser fields giving rise to a periodic standing wave potential of the form $V_{ol}(x) \equiv V \cos(2k_L x)$ with k_L denoting the optical lattice wave-number. In the mean field approximation, the system is described by a 1D Gross-Pitaevskii (GP) coupled equation for the two-component wave function, $\Psi_j \equiv \Psi_j(x, t)$, $j = 1, 2$,

$$i\hbar \frac{\partial \Psi_j}{\partial t} = \left[-\frac{\hbar^2}{2m_j} \frac{\partial^2}{\partial x^2} + V_{ol}(x) \right] \Psi_j + 2\hbar\omega_{\perp} (a_{jj} |\Psi_j|^2 + a_{j,3-j} |\Psi_{3-j}|^2) \Psi_j \quad (1)$$

where a_{jj} ($j = 1, 2$) and a_{12} are the two-body scattering lengths between intra- and inter-species of atoms. Eq. (1) can be put in dimensionless form by performing the following change of variables

$$x \rightarrow \frac{x}{k_L}, \quad t \rightarrow \frac{\hbar}{E_R} t, \quad V \rightarrow \frac{V}{E_R} \equiv V_0, \quad (2)$$

where space is measured in units of $1/k_L$, the energy in units of the lattice recoil energy $E_R \equiv \hbar\omega_R = \hbar^2 k_L^2 / 2\mu$ with $\mu = m_1 m_2 / (m_1 + m_2)$ the reduced mass, and time in units of \hbar/E_R , this leading to

$$i \frac{\partial \psi_j}{\partial t} = \left[-\epsilon_j \frac{\partial^2}{\partial x^2} + V_0 \cos(2x) \right] \psi_j + (g_j |\psi_j|^2 + g |\psi_{3-j}|^2) \psi_j, \quad j = 1, 2. \quad (3)$$

In the above equation the wavefunctions Ψ_j were rescaled according to

$$\Psi_j \equiv \sqrt{\frac{\omega_R}{2\omega_{\perp} a_0}} \psi_j(x, t) \quad (4)$$

and we denoted $\epsilon_j = \mu/m_j$, $j = 1, 2$, $g_j \equiv \frac{a_{jj}}{a_0}$, $g \equiv \frac{a_{j,3-j}}{a_0}$, with a_0 the background scattering length.

For deep optical lattices, e.g. when the OL amplitude is relatively large compared to E_R (say $V > 10E_R$ or $V_0 \gg 1$), it is possible to make the tight-binding approximation [15, 16] by expanding the two component wavefunctions ψ_j in terms of Wannier functions of the underlying linear periodic problem [17]

$$\psi_1(x, t) = \sum_n u_n(t) W_1(x - x_n), \quad \psi_2(x, t) = \sum_n v_n(t) W_2(x - x_n), \quad (5)$$

with time dependent expansion coefficients u_n, v_n to be fixed in such a manner that Eq. (3) is satisfied. By substituting the above expansions in Eq. (3) and using the orthonormality property of the Wannier functions $\int dx W_j(x - n)^* W_{j'}(x - n') = \delta_{j,j'} \delta_{n,n'}$, one gets the following coupled discrete nonlinear Schrödinger equations (DNLSE) [18]

$$i\dot{u}_n = -\kappa_1(u_{n+1} + u_{n-1}) - (\gamma_1 |u_n|^2 + \gamma_{12} |v_n|^2) u_n, \quad (6)$$

$$i\dot{v}_n = -\kappa_2(v_{n+1} + v_{n-1}) - (\gamma_{12} |u_n|^2 + \gamma_2 |v_n|^2) v_n,$$

where the overdot stands for time derivative. The coefficients κ_i , $i = 1, 2$, related to the tunneling rates of atoms between neighboring OL potential wells, and coefficients γ_j , $j = 1, 2$, related to the effective inter-species and intra-species nonlinearities, respectively, are expressed in terms of overlap integrals of Wannier functions as:

$$\begin{aligned} \kappa_j &= \epsilon_j \int W_j^*(x - n) \frac{\partial^2}{\partial x^2} W_j(x - (n + 1)) dx, \\ \gamma_j &= g_j \int dx |W_j(x - n)|^4, \quad j = 1, 2, \\ \gamma_{12} &= g \int dx |W_1(x - n)|^2 |W_2(x - n)|^2. \end{aligned} \quad (7)$$

Since the same OL acts on both components, the underlying linear periodic system is the same and so are the Wannier functions and corresponding tunneling coefficients, e.g.

$$\kappa_1 = \kappa_2 \equiv \kappa.$$

Notice that Eq. (6) has the Hamiltonian form $\dot{\chi}_n = \delta H / \delta \chi_n^*$ with $\chi_n = u_n, v_n$ and Hamiltonian H given by

$$H = - \sum_n \left[(\kappa_1 u_{n+1} u_n^* + \kappa_2 v_{n+1} v_n^* + c.c.) + \frac{1}{2} (\gamma_1 |u_n|^4 + \gamma_2 |v_n|^4) + \gamma_{12} |u_n|^2 |v_n|^2 \right]. \quad (8)$$

Here the star "*" stands for complex conjugation and *c.c.* denotes the complex conjugate of the expression in the parenthesis. In addition to the Hamiltonian (energy), the numbers of atoms $N_i = \sum_n |\chi_n|^2$, $\chi_n = u_n, v_n$ in each component are also conserved quantities. It is interesting to remark here that Eq. (6) also arises in nonlinear optics in connection with the propagation of the electric field in an array of optical waveguides with variable Kerr nonlinearity. In this context the role of time is played by the longitudinal propagation distance along the optical fiber and the nonlinear coefficients γ_{ij} correspond to self- and cross-phase modulations of the electric field components, respectively [19, 20].

In the following we consider BEC mixtures with fixed intra-species nonlinearities and subjected to periodic time modulations of the inter-species nonlinear parameter γ_{12} of the form

$$\gamma_{12}(t) \equiv \gamma_{12}^{(0)} + \gamma_{12}^{(1)}(t) = \gamma_{12}^{(0)} + \frac{\gamma_{12}^{(1)}}{\epsilon} \cos(\Omega \frac{t}{\epsilon}), \quad (9)$$

with $\gamma_{12}^{(0)}, \gamma_{12}^{(1)}$ real constants and ϵ a small parameter controlling the strongness of the modulation (SNM corresponds to $\epsilon \ll 1$ with $\Omega, \gamma_{12}^{(1)} \sim O(1)$). We remark that the choice in Eq. (9) of an harmonic modulating function of period $T = 2\pi/\Omega$ in the fast time variable $\tau = t/\epsilon$ is just for analytical convenience, what is important is the periodicity property of the modulation function rather than its shape, results being of general validity and can be easily extended to other types of periodic functions $\gamma_{12}^{(1)}(t)$. Periodic variations of the scattering length in time can be achieved by using the Feshbach resonance technique [21, 22]. This management setting is quite convenient in experiments since it involves only one parameter e.g. the inter-species scattering length (for the case of intra-species management see [6]). Moreover, the averaged equations obtained in the present case involve the coupling of the BEC components through the nonlinear dispersive terms that leads to novel types of binary compactons (see below).

To find effective nonlinear evolution equations, we use averaging method to eliminate the fast time, $\tau = t/\epsilon$, dependence. In this respect it is convenient to perform the following transformation

$$u_n = U_n e^{i\Gamma|V_n|^2}, \quad v_n = V_n e^{i\Gamma|U_n|^2}, \quad (10)$$

where Γ denotes the antiderivatives of $\gamma_{12}^{(1)}(t)$, e.g. $\Gamma_{12}(\tau) = \frac{\gamma_{12}^{(1)}}{\epsilon} \int_0^\tau \cos(\Omega\tau') d\tau'$. By substituting Eq. (10) into Eqs. (6) we obtain:

$$i\dot{U}_n = i\kappa_2 \Gamma(\tau) U_n [V_n^* X_1 - V_n X_1^*] - \kappa_1 X_2 - (\gamma_1 |U_n|^2 + \gamma_{12}^0 |V_n|^2) U_n, \quad (11)$$

$$i\dot{V}_n = i\kappa_1 \Gamma(\tau) V_n [U_n^* X_2 - U_n X_2^*] - \kappa_2 X_1 - (\gamma_2 |V_n|^2 + \gamma_{12}^0 |U_n|^2) V_n, \quad (12)$$

where $X_1 = U_{n+1}e^{i\Gamma\theta_1^+} + U_{n-1}e^{i\Gamma\theta_1^-}$, $X_2 = V_{n+1}e^{i\Gamma\theta_2^+} + V_{n-1}e^{i\Gamma\theta_2^-}$ and with θ_i^\pm denoting the quantities

$$\theta_1^\pm = |U_{n\pm 1}|^2 - |U_n|^2, \quad \theta_2^\pm = |V_{n\pm 1}|^2 - |V_n|^2. \quad (13)$$

The average over the rapid modulation can be easily done with the help of the following relations

$$\langle e^{\pm i\Gamma(\tau)\theta^\pm} \rangle = J_0(\alpha\theta^\pm), \quad \langle \Gamma(\tau)e^{\pm i\Gamma(\tau)\theta^\pm} \rangle = \pm i\alpha J_1(\alpha\theta^\pm), \quad (14)$$

where the angular bracket $\langle F \rangle$ denotes the average with respect to the fast time, e.g. $\langle F \rangle \equiv (1/T) \int_0^T F d\tau$, while J_0, J_1 are Bessel functions [23] of first kind of zero-th and first order, respectively, with the parameter α given by

$$\alpha = \gamma_{12}^{(1)}/\Omega. \quad (15)$$

The system of averaged equations is then obtained as:

$$\begin{aligned} i\dot{U}_n = & -\alpha\kappa_2 U_n \left[J_1(\alpha\theta_1^+) (V_n^* V_{n+1} + V_n V_{n+1}^*) + J_1(\alpha\theta_1^-) (V_n^* V_{n-1} + V_n V_{n-1}^*) \right] \\ & -\kappa_1 \left[U_{n+1} J_0(\alpha\theta_2^+) + U_{n-1} J_0(\alpha\theta_2^-) \right] - \left[\gamma_1 |U_n|^2 + \gamma_{12}^{(0)} |V_n|^2 \right] U_n, \end{aligned} \quad (16)$$

$$\begin{aligned} i\dot{V}_n = & -\alpha\kappa_1 V_n \left[J_1(\alpha\theta_2^+) (U_n^* U_{n+1} + U_n U_{n+1}^*) + J_1(\alpha\theta_2^-) (U_n^* U_{n-1} + U_n U_{n-1}^*) \right] \\ & -\kappa_2 \left[V_{n+1} J_0(\alpha\theta_1^+) + V_{n-1} J_0(\alpha\theta_1^-) \right] - \left[\gamma_2 |V_n|^2 + \gamma_{12}^{(0)} |U_n|^2 \right] V_n. \end{aligned} \quad (17)$$

Note that Eqs. (16, 17) have Hamiltonian form with averaged Hamiltonian H_{av} given by:

$$\begin{aligned} H_{av} = & - \sum_n \left[\kappa_1 J_0(\alpha\theta_2^+) [U_{n+1} U_n^* + c.c.] + \kappa_2 J_0(\alpha\theta_1^+) [V_{n+1} V_n^* + c.c.] \right. \\ & \left. + \frac{1}{2} (\gamma_1 |U_n|^4 + \gamma_2 |V_n|^4) + \gamma_{12}^{(0)} |U_n|^2 |V_n|^2 \right]. \end{aligned} \quad (18)$$

By comparing Eq. (18) with the corresponding unperturbed Hamiltonian Eq. (8), one can see that the effect of the inter-species scattering length modulation reflects in the following nonlinear rescaling of the tunneling constants:

$$\kappa_i \rightarrow \kappa_i J_0(\alpha\theta_{3-i}^+), \quad i = 1, 2. \quad (19)$$

Notice that, differently from the intra-species management considered in [6], the tunneling constant of one species depends on the difference of the atomic density between neighboring sites [9, 5] of the other species. This introduces nonlinear dispersive coupling terms in the averaged equations leading to novel types of two-component compactons. It is also worth to note here that the appearance of the Bessel functions in the above equations is a consequence of the choice of a sinusoidal modulation function. Compacton existence and lattice tunneling suppression, however, are independent on this. One can easily show that in the general case of a periodic (not sinusoidal) modulation of the scattering lengths, the above averaged equations will retain the same form except for the replacement of Bessel functions of the argument $\alpha\theta_i^\pm$ with more involved functions of the same arguments.

3. Exact binary compactons, stability analysis and numerical results

In this section we derive exact compacton solutions and study their stability properties both by standard linear analysis and by direct numerical integrations of the original nonlinear equations.

Exact compacton solutions of the averaged system can be searched in the form of stationary states

$$U_n = A_n e^{-i\mu_u t}, \quad V_n = B_n e^{-i\mu_v t}, \quad (20)$$

with μ_u, μ_v chemical potentials of the two atomic species.

By substituting these expressions into Eq. (16,17) one gets the following stationary equations:

$$\begin{aligned} \mu_u A_n + (\gamma_1 A_n^3 + \gamma_{12}^{(0)} B_n^2 A_n) + \kappa_1 [A_{n+1} J_0(\alpha\theta_2^+) + A_{n-1} J_0(\alpha\theta_2^-)] \\ + 2\alpha\kappa_2 A_n B_n [B_{n+1} J_1(\alpha\theta_1^+) + B_{n-1} J_1(\alpha\theta_1^-)] = 0, \end{aligned} \quad (21)$$

$$\begin{aligned} \mu_v B_n + (\gamma_2 B_n^3 + \gamma_{12}^{(0)} A_n^2 B_n) + \kappa_2 [B_{n+1} J_0(\alpha\theta_1^+) + B_{n-1} J_0(\alpha\theta_1^-)] \\ + 2\alpha\kappa_1 A_n B_n [A_{n+1} J_1(\alpha\theta_2^+) + A_{n-1} J_1(\alpha\theta_2^-)] = 0, \end{aligned} \quad (22)$$

to be solved for the chemical potentials and amplitudes A_n, B_n of the compacton modes.

To search for exact compactons one must look for the last sites of vanishing amplitude, say $n_0 \pm 1$, where the vanishing of the tunneling rate is realized. The compact nature of the solution ($A_i, B_i = 0$ outside a finite small range of sites), allows to reduce the above infinite system into a finite number of relations between the above variables, which can be solved exactly. This is shown explicitly below for different compacton types. For simplicity in the following we concentrate on bright-bright (B-B) solutions of the BEC mixtures. Similar results can be derived also for bright-dark and dark-dark compactons (omitted for brevity), in analogy to what done in Ref. [6] for the intra-species SNM case.

3.1. One-site compactons

A single site B-B compacton is achieved by assuming the following pattern for the amplitudes $A_{n_0} = a, B_{n_0} = b, A_{n_0 \pm j} = 0, B_{n_0 \pm j} = 0$ for all $j \geq 1$, with a, b real constants to be determined. Substituting this ansatz in Eqs.(21,22) we obtain the corresponding conditions for the compacton existence as

$$\begin{aligned} J_0(\alpha a^2) = 0, \quad a^2 = \xi_1/\alpha, \\ J_0(\alpha b^2) = 0, \quad b^2 = \xi_2/\alpha \end{aligned} \quad (23)$$

where ξ_1, ξ_2 are zeros (not necessary equal) of the Bessel function J_0 . This condition together with

$$\mu_u = -\gamma_1 a^2 - \gamma_{12} b^2, \quad \mu_v = -\gamma_2 b^2 - \gamma_{12} a^2 \quad (24)$$

gives us the single site B-B compacton pair. Typical examples of B-B compactons are shown in top panels of Fig. 1 together with their stability properties investigated

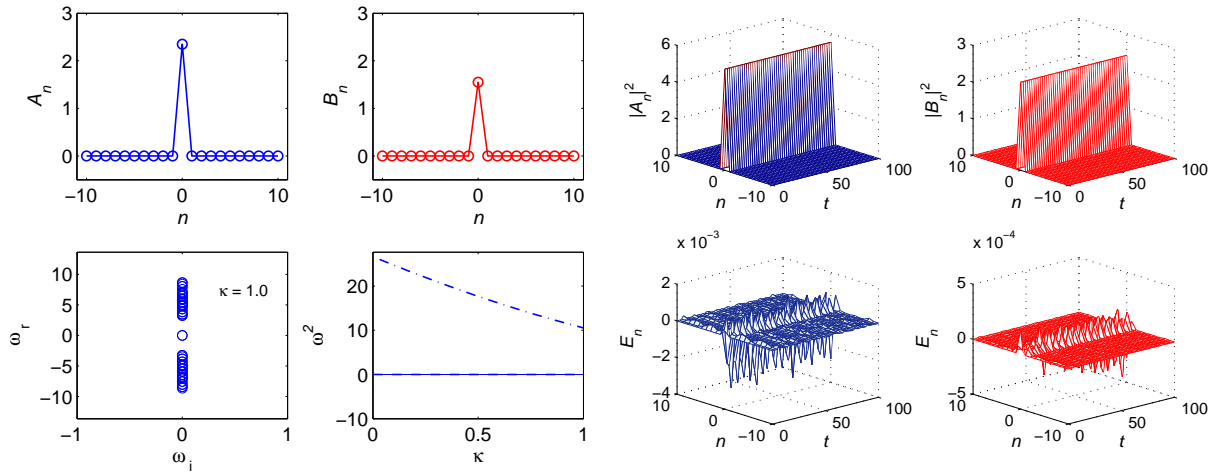


Figure 1. (Color online) Top panels. Exact single site B-B compacton of the averaged Eqs. (16-17) with first (first panel from the left) and second (second panel from the left) component amplitude fixed as $|A_0|^2 = 5.0074$ (second zero of J_0), $|B_0|^2 = 2.4048$ (first zero of J_0), respectively. Third and fourth top panels (from the left) show the space-time evolution of $|A_n|^2$ and $|B_n|^2$, respectively, as obtained from direct numerical integration of Eq. (6). Bottom panels. In the first panel (from the left) are shown the real and imaginary parts of the eigenfrequency ω of the linear system obtained by linearizing Eqs. (16-17) around the B-B compacton depicted in the top left panel, while in the second panel from the left are shown the lowest (solid line), third lowest (dash line), and fifth lowest (dash-dot line) ω^2 values as a function of the parameter κ . The remaining bottom panels show the time dependence of the deviations $E_n(t) \equiv |u_n(t) - u_n(0)|$, $E_n(t) \equiv |v_n(t) - v_n(0)|$, of the first (second panel from the right) and second (first panel from the right) component amplitudes depicted in the corresponding top panels, from their initial values at $t = 0$. In all the panels parameter values are fixed as: $\gamma_1 = \gamma_2 = 1$, $\gamma_{12}^{(0)} = 0.5$, $\kappa_1 = \kappa_2 \equiv \kappa = 1$ and $\alpha = 1$. The numerical integration of Eq. (6) is made by taking as initial condition the exact single site B-B compacton shown in the top left panel, the modulation function $\gamma_{12}(t) = \gamma_{12}^{(0)} + \frac{\alpha}{\epsilon} \cos(t/\epsilon)$, with $\epsilon = 0.01$ and all other parameters fixed as above.

by means of standard linear analysis performed on the averaged equation of motion. Denoting by ω the eigenfrequencies of the linearized averaged equations, associated with growing perturbation of the form $e^{-i\omega t}$, we have that linear stability is granted if all ω have zero imaginary parts. From the second row panels of Fig. 1 we see that one site B-B compactons are linearly very stable for a wide range of the parameter κ variation. Stability has been check also by direct numerical integrations of Eq. (6) shown in the two bottom panels of the figure.

3.2. Two-site compactons

Two-site B-B compactons also exist and, similarly to discrete breathers of binary non linear lattices [24], can be of three types: *in-phase*, *out-of-phase* and *mixed-symmetry* type, e.g. with both components symmetric (in-phase), or with both anti-symmetric

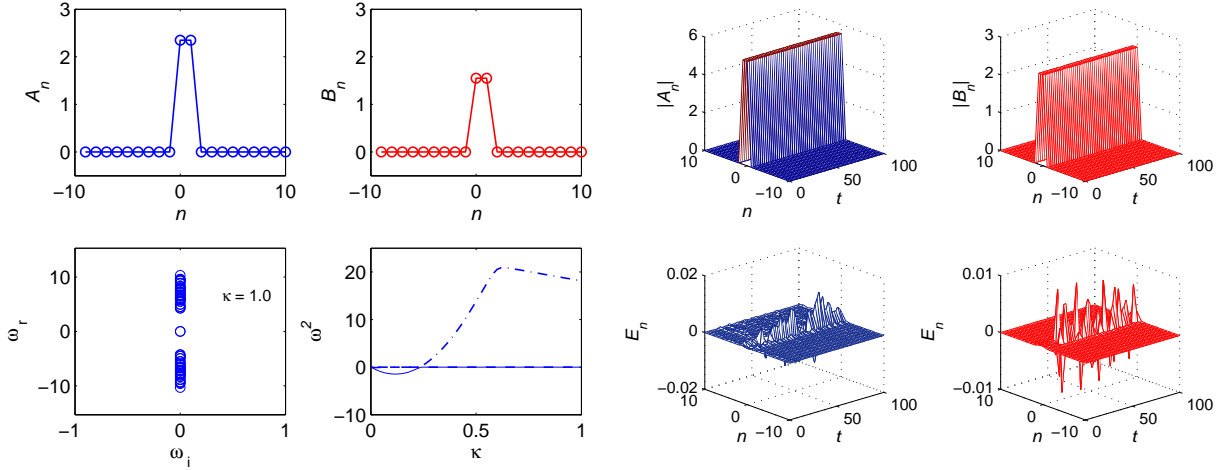


Figure 2. (Color online) Same as in Fig. 1 but for a two-site in-phase B-B compacton corresponding to the amplitude pattern given in Eq. (25) with a, b fixed as the square root of the second and first zero of the Bessel function J_0 , respectively.

(out-of phase), or with one component symmetric and the other anti-symmetric (mixed-symmetry) [24], with respect to the middle point between the two sites on which they are localized, respectively. Two-site B-B compactons directly follow from Eqs. (21, 22) by assuming one of the following patterns, depending on their symmetry:

$$A_{n_0} = a, \quad A_{n_0+1} = a, \quad B_{n_0} = b, \quad B_{n_0+1} = b, \quad (25)$$

$$A_{n_0} = a, \quad A_{n_0+1} = -a, \quad B_{n_0} = b, \quad B_{n_0+1} = -b, \quad (26)$$

$$A_{n_0} = a, \quad A_{n_0+1} = a, \quad B_{n_0} = b, \quad B_{n_0+1} = -b, \quad (27)$$

$$A_{n_0} = a, \quad A_{n_0+1} = -a, \quad B_{n_0} = b, \quad B_{n_0+1} = b, \quad (28)$$

and with $A_n = B_n = 0$ for all other sites $n \neq n_0, n_0 + 1$. Here the Eqs. (25) and (26) refer to the in-phase and out-of-phase compactons, respectively, while Eqs. (27) and (28) to compactons of mixed-symmetry type. By substituting the above expressions into Eqs.(21,22) one obtains the same condition in Eq. (23) as before, but with chemical potentials given by:

$$\begin{aligned} \mu_u &= -\gamma_1 a^2 - \gamma_{12}^{(0)} b^2 + \pm \kappa_1, \\ \mu_v &= -\gamma_2 b^2 - \gamma_{12}^{(0)} a^2 + \pm \kappa_2, \end{aligned} \quad (29)$$

where the combinations of signs, $(-, -)$, $(+, +)$ in front of the terms κ_1, κ_2 , refer to the in-phase and out-of-phase compactons, respectively, while the other combinations $(-, +)$ and $(+, -)$, refer to mixed-symmetry compactons in (27), (28), respectively.

Typical result for the in-phase and out-of-phase two-site B-B compactons are shown on Fig. 2 and in Fig. 3, respectively. We see that in both cases the excitations are very stable for a wide parameter range and the stability predicted by the linear analysis is corroborated by the direct numerical integrations of the original (unaveraged) system. Similar results are obtained also for two site compactons of mixed-symmetry type, but not shown here for brevity.

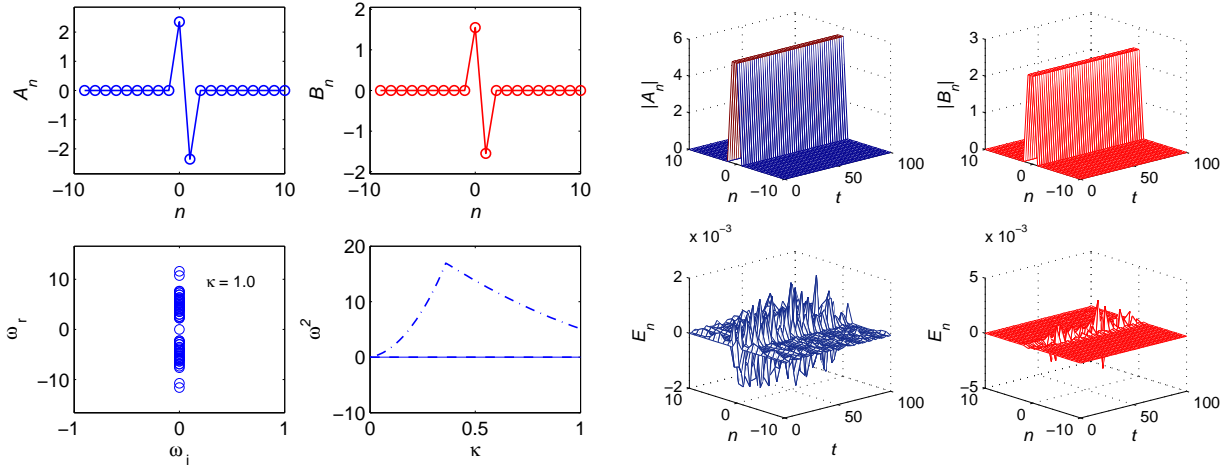


Figure 3. (Color online) Same as in Fig. 1 but for a two-site out-of-phase B-B compacton corresponding to the amplitude pattern given in Eq. (26) with a, b , fixed as the square root of the second and first zero of the Bessel function J_0 , respectively.

3.3. Three-sites compactons

Compactons of larger size can be found in similar manner. For example, we consider here only the case of three-site B-B compactons, corresponding to the pattern

$$\begin{aligned} A_{n_0} &= a_1, A_{n_0 \pm 1} = a_2, A_{n_0 \pm 2} = 0, \dots, \\ B_{n_0} &= b_1, B_{n_0 \pm 1} = b_2, B_{n_0 \pm 2} = 0, \dots, \end{aligned} \quad (30)$$

one finds the chemical potentials are given by

$$\begin{aligned} \mu_u &= -\gamma_1 a_2^2 - \gamma_{12}^{(0)} b_2^2 - \kappa_1 a_1 J_0(\xi_v) / a_2 - 2\alpha \kappa_2 b_1 b_2 J_1(\xi_v) \\ \mu_v &= -\gamma_2 b_2^2 - \gamma_{12}^{(0)} a_2^2 - \kappa_2 b_1 J_0(\xi_u) / b_2 - 2\alpha \kappa_1 a_1 a_2 J_1(\xi_u) \end{aligned}$$

with $\xi_u = \alpha(a_1^2 - a_2^2)$ and $\xi_v = \alpha(b_1^2 - b_2^2)$. The boundary amplitudes a_2, b_2 are given by the zero tunneling condition as in Eq. (23), e.g.

$$\begin{aligned} J_0(\alpha a_2^2) &= 0, \quad a_2^2 = \xi_1 / \alpha, \\ J_0(\alpha b_2^2) &= 0, \quad b_2^2 = \xi_2 / \alpha, \end{aligned} \quad (31)$$

and the central amplitudes a_1, b_1 , are obtained by solving the following equations:

$$\begin{aligned} a_1 a_2 \left[\gamma_1 (a_2^2 - a_1^2) + \gamma_{12}^{(0)} (b_2^2 - b_1^2) - 2\alpha \kappa_2 b_1 b_2 (2J_1(\alpha \xi_u) + J_1(\alpha \xi_v)) \right] \\ = \kappa_1 (a_2^2 - 2a_1^2) J_0(\xi_v), \end{aligned} \quad (32)$$

$$\begin{aligned} b_1 b_2 \left[\gamma_2 (b_2^2 - b_1^2) + \gamma_{12}^{(0)} (a_2^2 - a_1^2) - 2\alpha \kappa_1 a_1 a_2 (2J_1(\alpha \xi_v) + J_1(\alpha \xi_u)) \right] \\ = \kappa_2 (b_2^2 - 2b_1^2) J_0(\xi_u). \end{aligned} \quad (33)$$

Typical results for three-site B-B compactons are shown in Fig. 4.

Before closing this section, it is worth to we note that in spite of the different averaged equations, the existence conditions for one-site and two-site compacton are

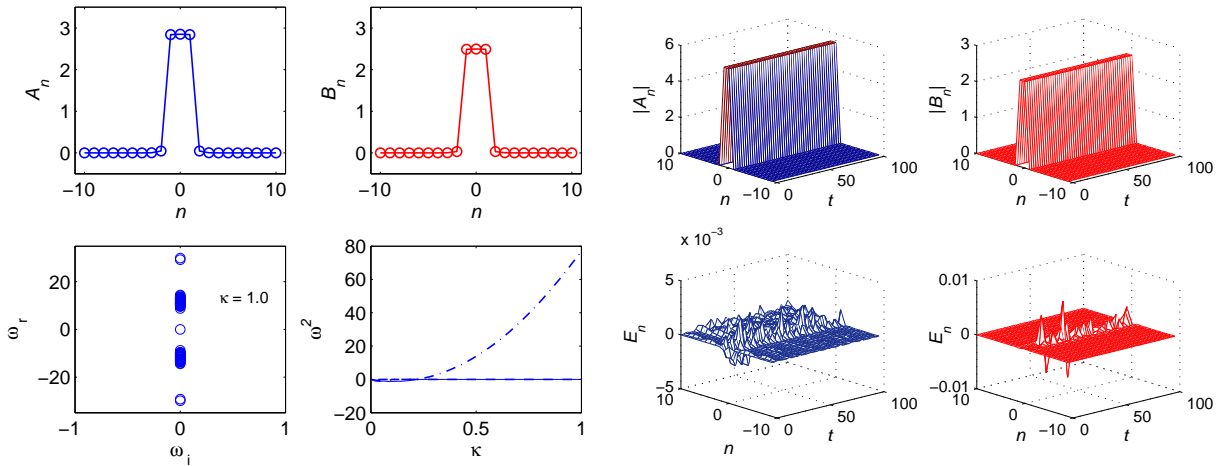


Figure 4. (Color online) Same as in Fig. 1 but for a three-site B-B compacton corresponding to the amplitude pattern given in Eq. (30) with a_2, b_2 , fixed as the square root of the third and fourth zero of the Bessel function J_0 , respectively, and with a_1, b_1 obtained from Eqs. as: $a_1 =, b_1 =$. All other parameters are fixed as in Fig. 1.

the same as for the the intra-species SNM case considered in Ref. [6]. This fact can be easily understood by noting that under the interchange of variables $\theta_1^+ \leftrightarrow \theta_2^+$ in the nonlinear dispersive part of the averaged Hamiltonian (18), and with the identification of parameters $\gamma_1, \gamma_2, \gamma_{12}^0$ with $\gamma_1^{(0)}, \gamma_2^{(0)}, \gamma_{12}$, respectively, the Hamiltonian in Eq. (18) reduces to the one of the intra-species SNM case considered in Ref. [6] (see Eq. (14) of Ref. [6]). Clearly, this transformation is invariant for one-site compactons because, due to the vanishing of the amplitudes at all sites $n \neq n_0$ (all the matter being localized on the site n_0), the nonlinear dispersive terms are automatically zero. This explain why the existence conditions for the single-site compactons are the same for inter- and intra-species SNM. A similar situation occurs also for two-site compactons because, due to the particular symmetry of the solutions, we have $\theta_1^+ = \theta_2^+ = 0$ and the above transformation is invariant for two-site compactons. In all other cases, however, e.g. for all compactons localized on more than two sites, the invariance is broken and the existence conditions are different for inter- and intra-species SNM cases. It should also be remarked here that since the averaged equations of motion for inter- and intra-species SNM cases are intrinsically different, stability properties of binary compactons will always be different (including one-site and two-site compactons) in the two SNM cases.

4. Stationary quasi-compactons under inter-species SNM

From the above analysis it follows that a necessary condition for exact stationary compactons to exist is that the BEC densities (multiplied by α) at the edges sites coincide with zeros of the Bessel function J_0 . This is obviously necessary for the zero tunneling condition in Eq. (23) to be satisfied and therefore for the suppression of any

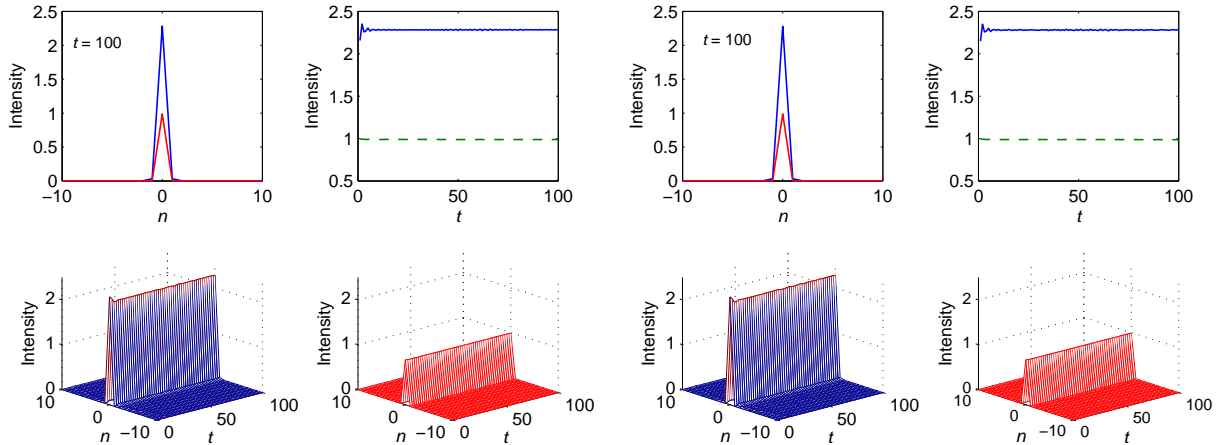


Figure 5. (Color online) Top panels. First (upper curve) and second (lower curve) component profiles of a single site B-B quasi-compacton at time $t = 100$ (first and third top panels from the left), and density time evolution at the middle site $n_0 = 0$ (second and fourth panel from the left), as obtained from numerical integrations of Eqs. (16,17) (first and second panels from the left) and of Eq. (6) (third and fourth panels from the left), respectively. Bottom panels shown the full time evolution of the quasi-compacton first and second components obtained from Eqs. (16,17) (first and second panels from the left) and from Eq. (6) (third and fourth panels from the left), respectively. In all panels the initial conditions were taken as $|A_0|^2 = 2.4048$ (first root of Bessel function), $|B_0|^2 = 1.0$ while the parameter values were fixed as $\gamma_1 = \gamma_2 = 1, \gamma_{12}^{(0)} = 1.0, \kappa_1 = \kappa_2 \equiv \kappa = 0.5$ and $\alpha_1 = \alpha_2 = 1$. The numerical integration of Eq. (6) is made with the same modulation function $\gamma_{12}(t)$ as in Fig. 1 but with $\epsilon = 0.005$.

tail in the solution. In the case of a single site compacton this implies that the numbers of atoms in the two components cannot be arbitrary but must be related by

$$\frac{N_1}{N_2} = \frac{\xi_1}{\xi_2} \quad (34)$$

with ξ_i two zeros (not necessarily equal) of J_0 . From this it also follows that for an exact binary compacton with a given number of particles N_1 in the first component, controlled by the parameter α , only a discrete set of values for N_2 are permitted.

On the other hand, it is also interesting to look for stationary quasi-compactons in which one of the two components amplitude (say the first) is associated to a zero of the Bessel function J_0 , while the other is not. In the following we report results obtained by direct numerical integrations of both the averaged Eqs. (16,17) and the original system Eq. (6), for specific choices of the (inexact) component and for different parameter values, with the interspecies interaction $\gamma_{12}^{(0)}$ typically varied in the range $0 \div 1.0$ (similar results are obtained for other choices of parameters). Notice that for the above setting, while the first component is initially taken as an exact compacton in the uncoupled limit $\gamma_{12}^{(0)} = 0$, the second component is inexact and therefore can not survive in absence of coupling (see Ref. [5] for the single component case).

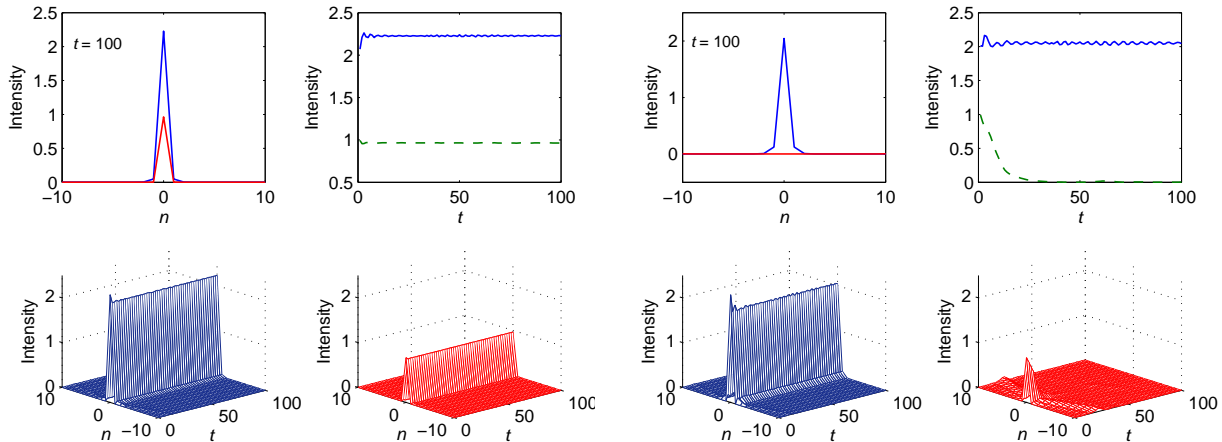


Figure 6. (Color online) First and second rows, repeating the same parameters as in Fig. 5 except $\gamma_{12} = 0.3$ and similarly for the third and the fourth rows but $\gamma_{12} = 0.2$. The results are obtained by solving the original Eq. (6).

In the top panels of Figs. 5, 6, are reported the profiles of the quasi-compacton components at the time $t = 100$ (first and third top panels from the left) together with their peak density at the middle sites time evolution (second and fourth top panels from the left), for the case $\gamma_{12} = 1.0$ in Fig. 5 and for the cases $\gamma_{12} = 0.3$ (first and second panels from the left) and $\gamma_{12} = 0.2$ (first and second panels from the right) in Fig. 6. As one can see, while in the first two cases the density at the middle site of the first component after an initial drop (due to matter emission) adjusts to a new practically constant value with small oscillations around it, and the density of the second component remains practically constant in time, in the last case (e.g. $\gamma_{12} = 0.2$) the second component cannot survive and quickly decays into background radiation. This is also clearly seen from the corresponding bottom panels showing the space-time evolution of the two BEC components. Actually this decay is associated to the occurrence of a delocalizing transition (see below) similar to the ones observed for single component BEC [25] and binary BEC mixtures in deep OL [26]. We also remark that in Fig. 5 the time evolutions are computed both with the averaged equations (first and second panels from the left) and with the original (unaveraged) system (first and second panels from the right), obtaining practically identical results. This is true for all numerically investigated cases provided the parameter ϵ is small enough (typically $\epsilon < 0.01$) for the SNM limit to be valid. In the following we remain strictly in this limit and report the time evolution only for one (averaged or original) system.

From Figs. 5, 6, we see that for fixed system parameters and initial conditions the existence of stable quasi-compactons crucially depends on the mean inter-species interaction parameter $\gamma_{12}^{(0)}$. More detailed investigations show that stable quasi-compactons exist in the SNM limit under very generic initial conditions (see below) provided the strength of the mean interspecies scattering length is above a critical

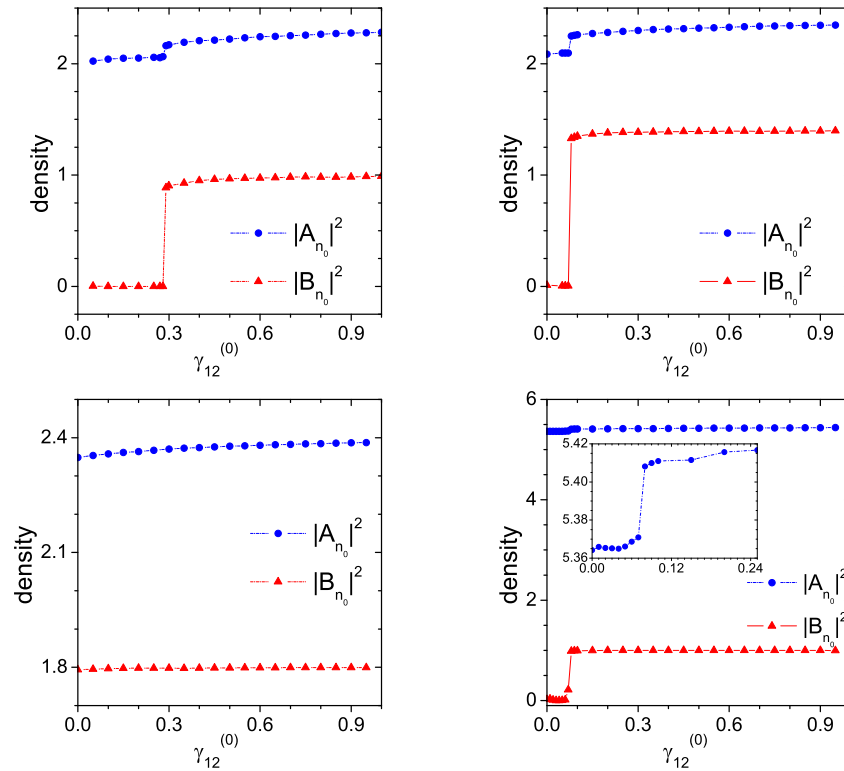


Figure 7. (Color online) Dependence on the parameter $\gamma_{12}^{(0)}$ of the first and second component densities $|A|^2, |B|^2$, respectively, at site n_0 taken at time $t = 300$, as obtained from direct numerical integrations of Eq. (6). In the top panels and in the bottom left panel the initial condition for the first component at site n_0 was taken as the first root ($|A_0|^2 = 2.4048$) of the J_0 Bessel function and zero elsewhere, while second components at site n_0 were fixed as $|B_0|^2 = 1.0$ (top left panel), $|B_0|^2 = 1.4$ (top right panel), $|B_0|^2 = 1.8$ (bottom left panel) and zero elsewhere. In the bottom right panel the initial condition was $|A_0|^2 = 5.52007$ (second zero of J_0) and $|B_0|^2 = 1.0$. The inset in this panel shows an enlargement of the delocalizing transition occurring in the first component near $\gamma_{12}^{(0)} \approx 0.075$ of the top curve. All symbols correspond to points computed numerically, joining lines being drawn just to guide eyes. Other parameters are fixed as in Fig. 5. To accelerate convergence to stationary quasi-compacton at $t = 300$, the dissipative function in (35) with $\eta = 5$ was used during the time evolution.

threshold. Moreover, this threshold disappears when the initial amplitudes are relatively close to zeros of J_0 . This can be seen from Figs. 7, 9, where the dependence of the BEC densities at the central site n_0 on the parameter $\gamma_{12}^{(0)}$ is reported. Calculations here were done by numerically solving the averaged equations of motion for different initial conditions, scanning $\gamma_{12}^{(0)}$ in the interval $0,1$ with typical increments of 0.1 (reduced to 0.01 close to the delocalizing transition) and by introducing dissipative boundary conditions to eliminate the emitted radiation from the system and accelerate convergence to stationary quasi-compactons. This was achieved by adding dissipative terms of the

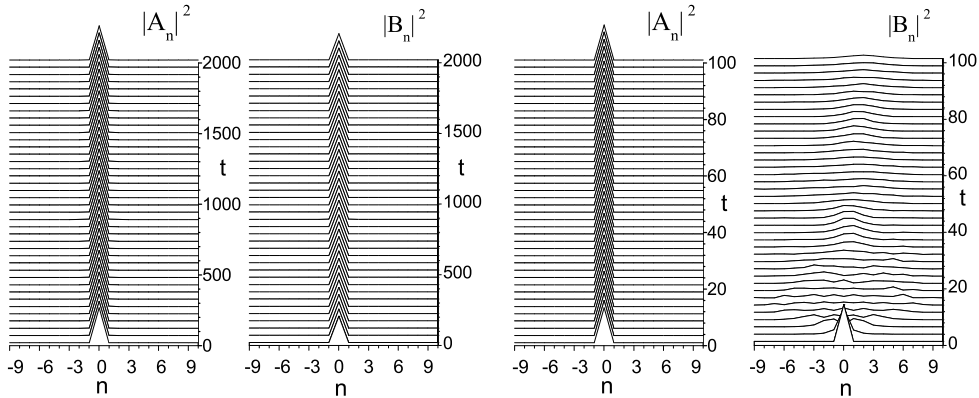


Figure 8. (Color online) Time evolution of a one-site quasi-compacton (first and second panel from the left) obtained from numerical integration of Eq. (6) with $\gamma_{12}^{(0)} = 0$ and initial conditions $|A_0|^2 = 2.4048$ (first root of Bessel function), $|B_0|^2 = 1.8$. Other parameters as fixed as for the bottom left panel Fig. 5. The right two panels show the corresponding time evolution for the intra-species SNM case, (Eqs. (12), (13) of Ref. [6]), with the same initial condition and parameters values as in the left two panels and with $\gamma_1^{(0)} \equiv \gamma_1 = 1.0$, $\gamma_2^{(0)} \equiv \gamma_2 = 1.0$, $\gamma_{12} \equiv \gamma_{12}^{(0)} = 0$.

form $i\xi_n u_n$, $i\xi_n v_n$ (resp. $i\xi_n U_n$, $i\xi_n V_n$) into the original (res. the averaged) equations for first and second component, respectively, with the function ξ_n taken as

$$\xi_n = \eta \operatorname{sech}^2(n - n_b), \quad (35)$$

with n_b denoting the boundary sites and the real parameter η controlling the strength of the dissipation. In all the panels of Fig. 7 the initial conditions for the first component were taken to satisfy the exact compacton zero tunneling condition in correspondence of the first (top panels and bottom left panel) and second (bottom right panel) zero of the Bessel function, while the second component was fixed as $|B_0|^2 = 1.0$ for top left and bottom right panels, and as $|B_0|^2 = 1.4$ and $|B_0|^2 = 1.8$ for the top right and bottom left panels, respectively. From the top left panel of Fig. 7 we see that a sharp transition (existence threshold) occurs at $\gamma_{12}^{(0)} \approx 0.29$. As the deviation of the inexact second component from the zero tunneling condition is reduced, keeping fixed all other parameters, the existence threshold moves toward a smaller value (see top right panel) and completely disappears when it is further reduced (see bottom left panel). For the considered parameters we find that the threshold disappears as the initial density of the second component at site n_0 become smaller than the critical value $|B_{cr}|^2 \approx 1.535$. Similar behaviors is observed also when the exact (first) component matches the zero tunneling condition at higher zeros of the Bessel function, as one can see from the bottom right panel of Fig. 7. In this case, however, note that the transition appears less sharp and also a bit more noisy in the tail, this being a consequence of the larger first component amplitude involved (see enlargement in the inset) and possibly also of the longer time required to converge to the solution.

From Fig. 7 it is also interesting to note that for relatively small initial deviations

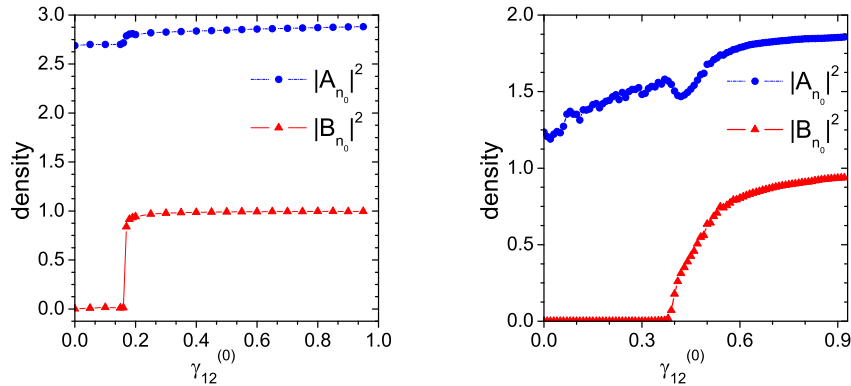


Figure 9. (Color online) Same as in Fig. 7 but for the case in which both components deviate from the exact zero tunneling condition. In the left and right panels the first component at central site n_0 was initially fixed as initial conditions at the central site were fixed as $|A_0|^2 = 3.0$ and $|A_0|^2 = 2.0$, respectively, and zero elsewhere, while the second component at site n_0 was fixed as $|B_0|^2 = 1.0$ for both panels, and zero elsewhere. All other parameters are the same as in Fig. 5.

from exact zero tunneling conditions there are no delocalizing transitions and it is possible to have quasi-compactons even when the inter-species mean scattering length is detuned to zero: $\gamma_{12}^{(0)} = 0$. In this case it is interesting to compare the quasi-compacton time evolution obtained from the inter- and intra-species SNM, using the same initial conditions and parameter values for the two cases. This is done in Fig. 8 from which we see that the lacking of nonlinear dispersion coupling makes impossible to sustain the quasi-compacton in the intra-species SNM case.

Finally, in Fig. 9 we investigate the case in which both components deviate from the exact zero tunneling conditions. As one can see, quasi-compactons exist also in this case but existence thresholds and sharpness of the delocalizing transition depend much more on how the deviations of the initial conditions from the exact zero tunneling condition are taken. In the left panel of the figure it is shown the case in which the first component density is above the first zero of the Bessel function and the second component is below (e.g. $|A_0|^2 = 3.0$, $|B_0|^2 = 1.0$), while in the right panel the case in which both components smaller than the first zero of the Bessel function (e.g. $|A_0|^2 = 2.0$, $|B_0|^2 = 1.0$). We see that in the first case the transition is sharp and similar to the ones shown in Fig. 7, while in the second case the transition is not sharp and very noisy with both components dropping from their initial values much more (due to a larger emitted background radiation adsorbed, in our simulation, at the ends of the chain). Quite remarkably, also in this case quasi-compacton survive on a very long time scale similarly to the binary compacton shown in the first two left panels of Fig. 9.

5. Discussion and Conclusions

Before closing this paper let us discuss conditions for possible experimental observation of the above results. Example of boson-boson mixtures which can be considered are ^{39}K - ^{87}Rb , ^{41}K - ^{87}Rb , ^{85}Rb - ^{87}Rb . At the present binary BEC mixtures are observed for the system ^{85}Rb - ^{87}Rb [27] and ^{41}K - ^{87}Rb [28]. The inter-species scattering length can be varied in time by means of the Feshbach resonance technics.

Possible experimental implementations of the results discussed in this paper could be made by considering ^{85}Rb - ^{87}Rb boson-boson mixtures loaded in the deep optical lattices [27, 29, 30]. The inter-species scattering length can be varied in time by means of the Feshbach resonance technics (see the recent review [22] and references therein). In this case the variation the inter-species scattering length a_{12} can be described by the formula

$$a_{12} = a_{bg} \left(1 - \frac{\Delta}{B - B_R} \right), \quad (36)$$

with a_{bg} denoting the background scattering length, e.g. the one far from the resonance, B_R the resonance position where the scattering length diverges, and Δ the resonance width [22]. By assuming an external time dependent magnetic field of the form: $B(t) = B_R + \Delta + \delta + B_1 \cos(\omega t)$, with B_1 a constant amplitude and δ denoting the detuning from the zero crossing point of the scattering length, occurring at $B_R + \Delta$. Introducing the parameters $\alpha = \delta/\Delta$ and $\beta = B_1/\Delta$, we have

$$\frac{a_{12}}{a_{bg}} = \frac{\alpha + \beta \cos(\omega t)}{1 + \alpha + \beta \cos(\omega t)} = a_0 + a_1 \cos(\omega t) + a_2 \cos(2\omega t) + \dots \quad (37)$$

By referring to the ^{41}K - ^{87}Rb BEC mixture, two Feshbach resonances exist, one at 35G and the other at 79G [29]. Considering the resonance at $B_R = 35\text{G}$, we have $\Delta = (5.1 \pm 1.8)\text{G}$ with a background scattering length $a_{bg} \approx 500a_B$, where $a_B = 0.0529\text{nm}$ is the Bohr radius. By assuming $\Delta = 5.1\text{G}$, $\delta = 0.08\text{G}$, $B_1 = 1.25\text{G}$, we have $\alpha = 0.016$, $\beta = 0.25$ and the first Fourier coefficients in Eq. (37) are readily estimated as $a_0 \approx -0.0154$, $a_1 \approx 0.2538$, $a_2 \approx 0.0317$, $a_3 \approx 0.00396217$. From the numerical calculations of the averages in Eq. (14), one can check that all higher harmonics give negligibly contribution to the averaged equations, so that, for any practical purpose, the effective inter-species modulation for the chosen parameters can be taken as in Eq. (9). Finally, we remark that the optical lattice parameters can be fixed according to the experiment [30], e.g., $\lambda_L = 1064\text{nm}$, with $V_0/E_R > 10$, to guarantee the validity of the tight-binding approximation [15, 16, 17].

In the SNM limit we expect compactons to be elementary excitations of the binary BEC system and as such they should emerge spontaneously from generic initial conditions. For compactons detection in real experiments, therefore, one could start from generic localized matter wave-packet and observe their decomposition into compacton modes localized on few optical lattice during the time evolution. An example of this is shown in Fig. 10 where we have numerically simulated a three-site binary compacton formation starting from initial gaussian profiles for the two components. We

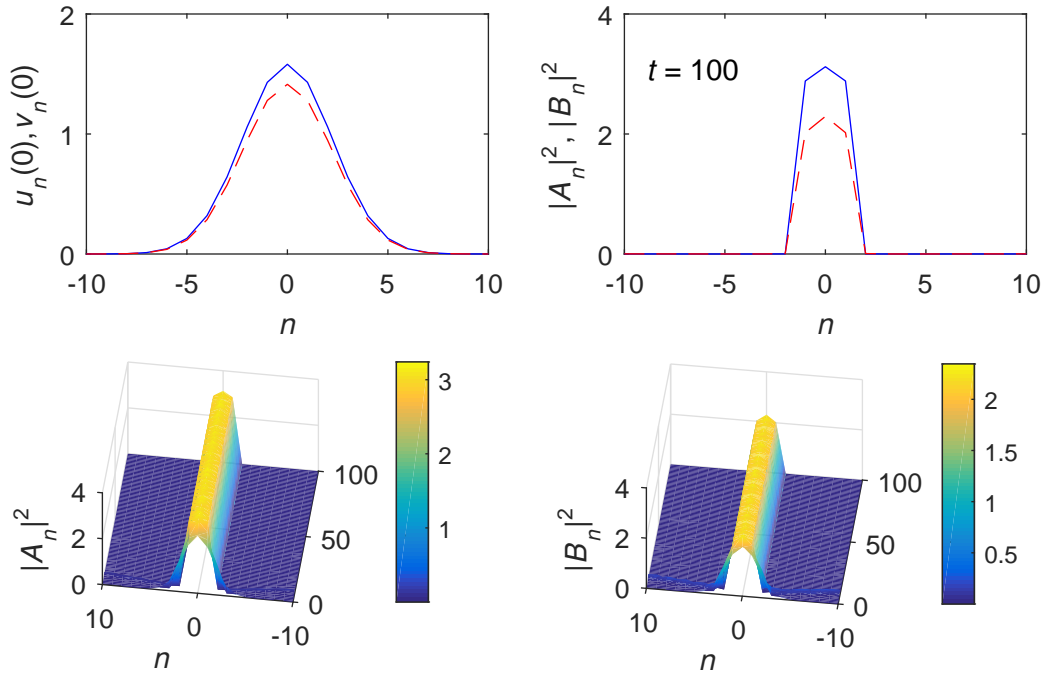


Figure 10. (Color online) Top left panel. Initial Gaussian profiles $u_n(0) = \sqrt{2.5}e^{-0.1n^2}$ (solid line) and $v_n(0) = \sqrt{2.0}e^{-0.1n^2}$ (dash line) and at the right, the amplitudes at $t = 100$ which are practically three-sites compactons. Other parameters are fixed as in Fig. 5. Bottom plots show the transient amplitudes along the time interval. To eliminate the matter radiation generated during the time evolution, the absorbing boundary conditions with the function ξ_n as in (35) with $\eta = 10$, was used.

see that the emitted radiation can be very small if the initial conditions are properly prepared (the numbers of atoms should be close to the ones theoretically predicted for compacton existence discussed in section 3. For fixed parameters and qualitatively similar initial conditions, one should observe delocalization transitions [25] occurring in one or in both components, that are very sharp or quite broad, depending on how the initial condition were prepared, as the inter-species scattering length is varied across the threshold value (see section 4).

In conclusion, we have investigated in this paper the existence and stability of compactons and quasi-compactons of binary BEC mixtures trapped in deep OL, induced by periodic time modulations of the inter-species scattering length. We showed that in the SNM limit exact stationary compactons exist when the numbers of atoms in the two components are related in a precise manner by a zero tunneling condition at the excitation edges. Slightly deviations from these conditions give rise to quasi-compactons, e.g. to solutions for which the zero tunneling condition and the localization on a compact is not exact but achieved dynamically through the coupling induced by the scattering length modulation. Stability properties of stationary compactons and quasi-compactons have been extensively investigated both by linear analysis (for exact compactons) and

by direct numerical integrations both of the averaged equations and of the original systems (compactons and quasi compactons cases). The comparison between analytical and numerical results are found in excellent agreement and confirm that compactons and quasi-compactons are very robust and stable excitations. This particularly true for inter-species scattering length that, for fixed parameters and initial conditions, are above the existence thresholds. Possible parameter designs and experimental settings for BEC compactons observation was also discussed.

Acknowledgements

M. S. acknowledges partial support from the Ministero dell'Istruzione, dell'Università e della Ricerca (MIUR) through the PRIN (Programmi di Ricerca Scientifica di Rilevante Interesse Nazionale) grant on "Statistical Mechanics and Complexity": PRIN-2015-K7KK8L. F.A, M.A.S.H., and B.A.U. acknowledges the support from the grant of MHE(Malaysia): FRGS16-013-0512.

- [1] Rosenau R, Hyman J M 1993 *Phys. Rev. Lett.* 1993 **70**, 564; Rosenau P *Phys. Rev. Lett.* 1994 **73** 1737.
- [2] Rosenau P. and Kashdan E 2008 *Phys. Rev. Lett.* **101**, 264101 Rosenau P. and Kashdan E 2010 *Phys. Rev. Lett.* **104**, 034101.
- [3] Pikovsky A and Rosenau P 2006 *Physica D* **218**, 56.
- [4] Johansson M, Naether U, and Vicencio R 2014 *Phys. Rev. E* **92**, 032912.
- [5] Abdullaev F Kh, Kevrekidis P G, and Salerno M 2010 *Phys. Rev. Lett.* **105**, 113901.
- [6] Abdullaev F Kh, Hadi M S A, Salerno M, and Umarov B A 2014 *Phys. Rev. A* **90**, 063637.
- [7] D' Ambroise J, Salerno M, Kevrekidis P, and Abdullaev F Kh 2015 *Phys. Rev. A* **92**, 053621.
- [8] Abdullaev F Kh and Kraenkel R A 2000 *Physics Letters A* **272**, 395.
- [9] Gong J, Morales-Molina L, and Hänggi P 2009 *Phys. Rev. Lett.* **103**, 133002.
- [10] Meinert F, Mark M J, Lauber K, Daley A J, and Nagerl H-C 2016 *Phys. Rev. Lett.* **116**, 205301.
- [11] Greschner S, Sun G, Poletti D, Santos L 2014 *Phys. Rev. Lett.* **113**, 215303.
- [12] Rapp A, Deng X, and Santos L 2012 *Phys. Rev. Lett.* **109**, 203005.
- [13] Wang T, et al. 2014 *Phys. Rev. A* **90** 013633.
- [14] Greschner S, Santos L, Poletti D 2014 *Phys. Rev. Lett.* **113**, 183002.
- [15] Trombettoni A and Smerzi A 2001 *Phys. Rev. Lett.* **86**, 2353.
- [16] Abdullaev F Kh, Baizakov B B, Darmanyan S A, Konotop V V, and Salerno M, 2001 *Phys. Rev. A* **64**, 043606.
- [17] Alfimov G L, Kevrekidis P G, Konotop V V, and Salerno M 2002 *Phys. Rev. E* **66** 046608.
- [18] Shrestha U, Javanainen J, and Ruostekoski J 2009 *Phys. Rev. Lett.* **103**, 190401.
- [19] Kobayakov A, Darmanyan S, Lederer F, Schmidt E 1998 *Optical and Quantum Electronics* **30**, 795.
- [20] Assanto G, Cisneros L A, Minzonni A A, Skuse B D, Smyth N F, and Worthy A L 2010 *Phys. Rev. Lett.* **104**, 053903.
- [21] Inouye S, Andrews M R, Stenger J, Miesner H -J, Stamper-Kurn D M and Ketterle W 1998 *Nature* **392**, 151.
- [22] C. Chin, R. Grimm, P. Julienne, and E. Tiesinga, *Rev. Mod. Phys.* 82, 1225 (2010).
- [23] Abramowitz M and Stegun I A, 1964 *Handbook of Mathematical Functions*, (National Bureau of Standards, Washington).
- [24] H.A. Cruz, V.A. Brazhnyi, V.V. Konotop, G.L. Alfimov, and M. Salerno, 2007 *Phys. Rev. A* **76** 013603-1-14.
- [25] B.B. Baizakov and M. Salerno, *Phys. Rev. A* **69** (2004) 013602.

- [26] H.A. Cruz, V.A. Brazhnyi, V.V. Konotop, and M. Salerno, *Physica D* **238** 1372-1387.
- [27] Papp S B, Pino J M, and Wieman C E 2008 *Phys. Rev. Lett.* **101**, 040402.
- [28] Modugno G, Modugno M, Riboli F, Roati G, and Inguscio M, 2002 *Phys. Rev. Lett.* **89**, 190404.
- [29] Thalhammer G et al. 2008 *Phys. Rev. Lett.* **100**, 210402.
- [30] Catani J et al. 2008 *Phys.Rev. A* **77**, 011603(R).